Amygdala GABA Neurons: Gatekeepers of Stress and Reproduction

Author Information

Affiliations

[1]Department of Women and Children's Health, School of Life Course and Population Sciences, King's College London, Guy's Campus, London SE1 1UL, UK and [2]Department of Mathematics and Statistics, [3]Living Systems Institute, [4]Biological Sciences, University of Missouri, Columbia, MO 65211-7400 and [5]EPSRC Hub for Quantitative Modelling in Healthcare, University of Exeter, Stocker Road, Exeter EX4 4PY, UK

Junru Yu,[1,†] Saeed Farjami,[2,3,†] Kateryna Nechyporenko,[2,3,†] Xiao Feng Li,[1]

Hafsa Yaseen,[1,4] Yanyan Lin,[1] Jinbin Ye,[1] Owen Hollings,[1] Kevin T. O'Byrne,[1,*] Krasimira Tsaneva-Atanasova,[2,3,5,*] Margaritis Voliotis,[2,3,*]

Contributions

J.Y. contributed data acquisition and data analysis, S.F. contributed data analysis, K.N. contributed modelling, M.V. contributed managing data analysis, X.F.L. contributed managing data acquisition, H.Y. contributed data acquisition, Y.L. contributed data acquisition, J.Y. contributed data acquisition, O.H. contributed data acquisition, K.T.O. and K.T.A. contributed to managing the project. All authors contributed to writing the manuscript.

Corresponding author

Correspondence to: Krasimira Tsaneva-Atanasova (K.Tsaneva-Atanasova@exeter.ac.uk), Kevin T. O'Byrne (kevin.o'byrne@kcl.ac.uk).

Abstract

Stress causes menstrual disturbances, infertility and other reproductive disorders. The posterodorsal medial amygdala (MePD) not only processes stress signals but is a critical modulator of the gonadotropin-releasing-hormone (GnRH) pulse generator, via GABAergic inhibitory projections to the hypothalamus. However, the mechanisms by which stress is processed within the MePD, particularly via the high density of GABAergic and Urocortin-3 (UCN3) neurons, remain poorly understood. Here, we combine *in-vivo* GRadient-INdex (GRIN) lens mini-endoscopic calcium imaging (proxy for neuronal activity) with optogenetics and computational modelling to elucidate the underlying circuitry and its dynamics. Our results reveal two anti-correlated GABAergic subpopulations in the MePD that dictate responses to both UCN3 neuron stimulation and restraint stress. Our computational model attributes the anti-correlated activity to mutually inhibitory interactions between the two GABAergic subpopulations and predicts how these interactions shape downstream-responses to stimulation of GABAergic and UCN3 neurons. We test these predictions using optogenetics and show that GABAergic neurons operate downstream of the UCN3 population, playing a critical role in relaying UCN3 signals to modulate LH pulse frequency. Our study demonstrates for the first time how GABAergic neurons in the amygdala regulate the effects of stress on reproductive functions, revealing key neural mechanisms that link emotional and reproductive health.

Introduction

Successful reproduction requires normal function of a neural oscillator, the gonadotrophin-releasing hormone (GnRH) pulse generator, that drives the pulsatile release of gonadotropic hormones, luteinising hormone (LH) and follicle stimulating hormone (FSH) to control ovulation and spermatogenesis. This oscillator comprises Kisspeptin neurons co-expressing Neurokinin-B (NKB) and Dynorphin A (acronym KNDy) in the hypothalamic arcuate nucleus (ARC). The KNDy neural network not only provides the essential episodic stimulatory kisspeptin signal to the GnRH neurons, but receives diverse afferent inputs and hence is a hub for integrating various internal and external cues that regulate reproductive function[1,2].

The most common cause of insufficient GnRH drive is functional, that is, due to neuroendocrine effects of psychological and behavioural variables.

The amygdala, a part of the limbic brain typically associated with emotions and anxiety, has strong projections to the KNDy system[1,2]. The medial amygdala, and more specifically its posterodorsal subnucleus (MePD), has been shown to be a robust upstream regulator of GnRH pulse generator frequency[3–5], pubertal timing[6,7], sociosexual behaviour[8,9], anxiety[8] and psychological stress-induced suppression of pulsatile LH secretion[10,11].

In the MePD, over 66% of neurons are GABAergic and make up about 80% of its projections, many to key hypothalamic reproductive centres[12], including the KNDy neurons and optogenetic stimulation of the latter suppress LH pulsatility[11]. Moreover, chemogenetic inhibition of GABA neurons in the MePD can reverse the inhibitory effect of psychogenic stress on LH pulsatility[11], suggesting an involvement of GABAergic signalling in the stress-induced suppression of pulsatile LH secretion. Although the precise way in which the MePD GABAergic neurons influence LH pulsatility is not fully understood, it has been suggested that they interact with the stress neuropeptide urocortin-3 (UCN3) neurons to modulate or reinforce stress-induced suppression of LH pulse frequency.

UCN3, part of the of corticotropin-releasing factor (CRF) superfamily and selective for CRF type 2 receptors (CRFR2)[13], is highly expressed in the MePD[14,15]. Furthermore, UCN3 neurons in the MePD mediate psychosocial stress-induced suppression of the GnRH pulse generator and corticosterone secretion, thus play a central role in the interaction between the reproductive and stress axes[10,15]. Previously we have shown that intra-MePD GABA antagonism can reverse UCN3-induced LH pulse suppression[15], suggesting that GABA acts downstream of UCN3 signalling within the MePD. However, the local neural circuitry within the MePD mediating stress related information to the GnRH pulse generator remains to be established.

Here, we employed GRadient INdex (GRIN) lens mini-endoscopy to monitor the calcium activity of GABA neurons at single-cell resolution under acute psychological stress or optical stimulation of UCN3 neurons. Clustering analysis of the observed calcium transients uncovered two distinct GABAergic sub-populations

exhibiting anti-correlated activity. To explore the functional role of these two subpopulations and unpick the mechanisms driving their anti-correlated activity, we build upon our previously developed MePD circuitry mathematical modelling framework[5]. Our modelling reveals that mutual inhibitory interactions between the GABAergic populations are sufficient to drive anti-correlated activity and predicted a complementary inhibitory effect of GABA and UCN3 signalling on the frequency of the GnRH pulse generator, which we tested using an intersectional genetic strategy. Hence, by uncovering how subpopulations of MePD GABA neurons interact with UCN3 neurons to transmit stress information to the GnRH pulse generator we provide new insights into the underlying neural mechanisms of stress related reproductive disorders.

Results

Dynamic reconfiguration of MePD GABA neuronal networks during selective optical stimulation of UCN3 neurons and restraint stress

To investigate how the posterodorsal subnucleus of the medial amygdala (MePD) processes stress signals and to understand the role of GABAergic and UCN3 neurons in this process, we employed *in-vivo* calcium imaging using GRadient INdex (GRIN) mini-endoscopy. A cohort of six female UCN3-Cre::VGAT-Flpo transgenic mice were injected with a viral mixture containing pAAV-Syn-Flex-rc[Chrimson-tdTomato] and pAAV-EF1a-fDIO-GCaMP6s. This intersectional viral strategy enabled dual functionality: (i) optogenetically stimulating MePD UCN3 neurons via Chrimson; and (ii) detecting calcium activity in MePD GABAergic neurons using GCaMP6s (Fig. 1**A**). GRIN lenses were surgically implanted at the same location as the viral injection, enabling imaging of calcium activity with single-neuron resolution.

Two series of experiments were conducted to assess GABAergic responses under distinct conditions. First, to assess the role of UCN3 neurons in recruiting GABAergic response, baseline calcium activity from MePD GABAergic neurons was recorded for 2 min, followed by 2 min of recording during optogenetic stimulation of UCN3 neurons (Fig. 1**A**). Optical stimulation was delivered in a discontinuous pattern, 5 seconds on, 5 seconds off, with a light-pulse frequency of 10 Hz during the ‘on’ periods (10-ms pulse width, 10 mW power, and 532 nm wavelength). Furthermore, to further characterise the GABAergic

response to acute stressors, baseline calcium activity of GABAergic neurons was recorded for 2 min, followed by 2 min of recording while the animals were exposed to restraint stress (Fig. 1**A**).

The dynamic GABAergic response to optogenetic stimulation of UCN3 neurons and restraint stress was summarised in functional terms using pairwise (neuron-neuron) association matrices, constructed using the signed lagged cross-correlation (SLxCorr) metric. SLxCorr captures the correlation between the activity of two neurons while accounting for both temporal lags and the sign (positive or negative) of their association (see Methods). Hence, SLxCorr matrices represent the MePD GABAergic response as a set of interconnected nodes (neurons) with connections weighted by their functional interactions (Fig. 1**H**&**I**). Our analysis revealed significant differences in the functional connectivity of the GABAergic network in both experimental conditions (Fig. 1**J**). These results indicate that the GABAergic population in the MePD plays a pivotal role in processing stress signals, such as those induced by restraint stress. Furthermore, our findings suggest that UCN3 neurons may serve as a critical relay, transmitting stress-related information to the GABAergic population.

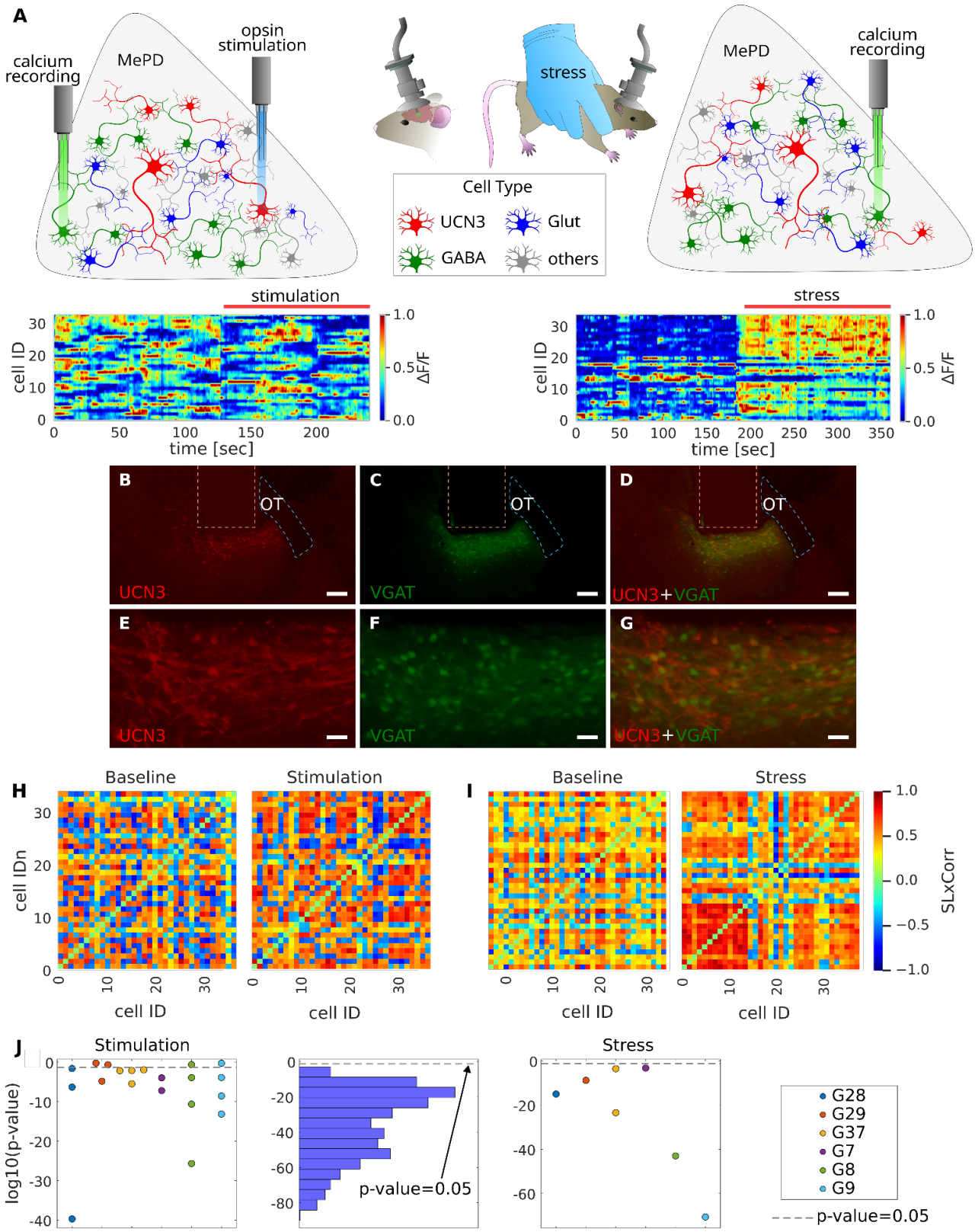

Figure 1: **Functional connectivity of GABAergic neurons in posterodorsal medial amygdala (MePD) reconfigures in response to optical stimulation of urocortin-3 (UCN3) neurons or acute restraint stress**. (**A**)

Schematic diagram of the experimental design for optically stimulating MePD UCN3 neurons and simultaneously imaging calcium activity from MePD GABAergic neurons. Heatmaps of calcium activity (ΔF/F) in response to (left) optical stimulation of UCN3 neurons and (right) during restraint-induced stress. (**B-G**) Representative photomicrographs of the MePD from a UCN3-Cre::VGAT-Flpo mouse injected with pAAV-Syn-Flex-rc+pAAV-EF1a-fDIO-GCaMP6s. (**B&E**) Red fluorescence (tdTomoato) labels UCN3 neurons expressing Chrimson-tdTomato, (**C&F**) green fluorescence labels GABAergic neurons, and (**D&G**) red and green signals merged. (**H&I**) Functional connectivity in the GABA populations was quantified using signed lagged cross-correlation (SLxCorr). (**J**) Functional connectivity matrices show a statistically significant difference between the baseline period and subsequent UCN3 stimulation or restraint stress across animals, assessed via Kolmogorov-Smirnov tests for each animal trial and using Fisher's method for combining p-values across different animals (see Methods). Distribution of combined p-value obtained from different combinations of trials (one from each animal) is consistently below the 0.05 confidence level. Scale bars: B-D, 200μm; E-G, 50μm.

Clustering analysis reveals two functionally distinct GABAegic sub-populations in the MePD

To better understand the functional organisation of the GABAergic MePD network during optical stimulation of UCN3 neurons and under restraint stress, we performed clustering analysis of the calcium recordings from GABAergic neurons.

The Signed Lagged Cross-Correlation (SLxCorr) was used as a distance metric, based on which we performed hierarchical clustering. Clustering results consistently revealed two functionally distinct cell populations both during optical stimulation of UCN3 neurons and restraint stress (Fig. 2**A**&**C**). Under both conditions, activity between the two clusters appeared highly anti-correlated as illustrated by two representative examples depicted in Fig. 2**B**&**D**. Moreover, we find that clusters are significantly different in size with the smallest cluster accounting on average for 35% of all cells (Fig 2**D**&**E**). The robustness of the above finding was also verified using the K-means clustering algorithm and pairwise covariance as an alternative distance metric (see Methods).

Based on the functional role of the MePD in relaying stress signals to the hypothalamic arcuate nucleus (ARC), our results suggest that the identified GABAergic subpopulations (clusters) could correspond to distinct populations of GABA interneurons and GABA efferent neurons projecting to the ARC. These

projections play a role in regulating the gonadotropin-releasing hormone (GnRH) pulse generator, a key driver of reproductive function[5,11].

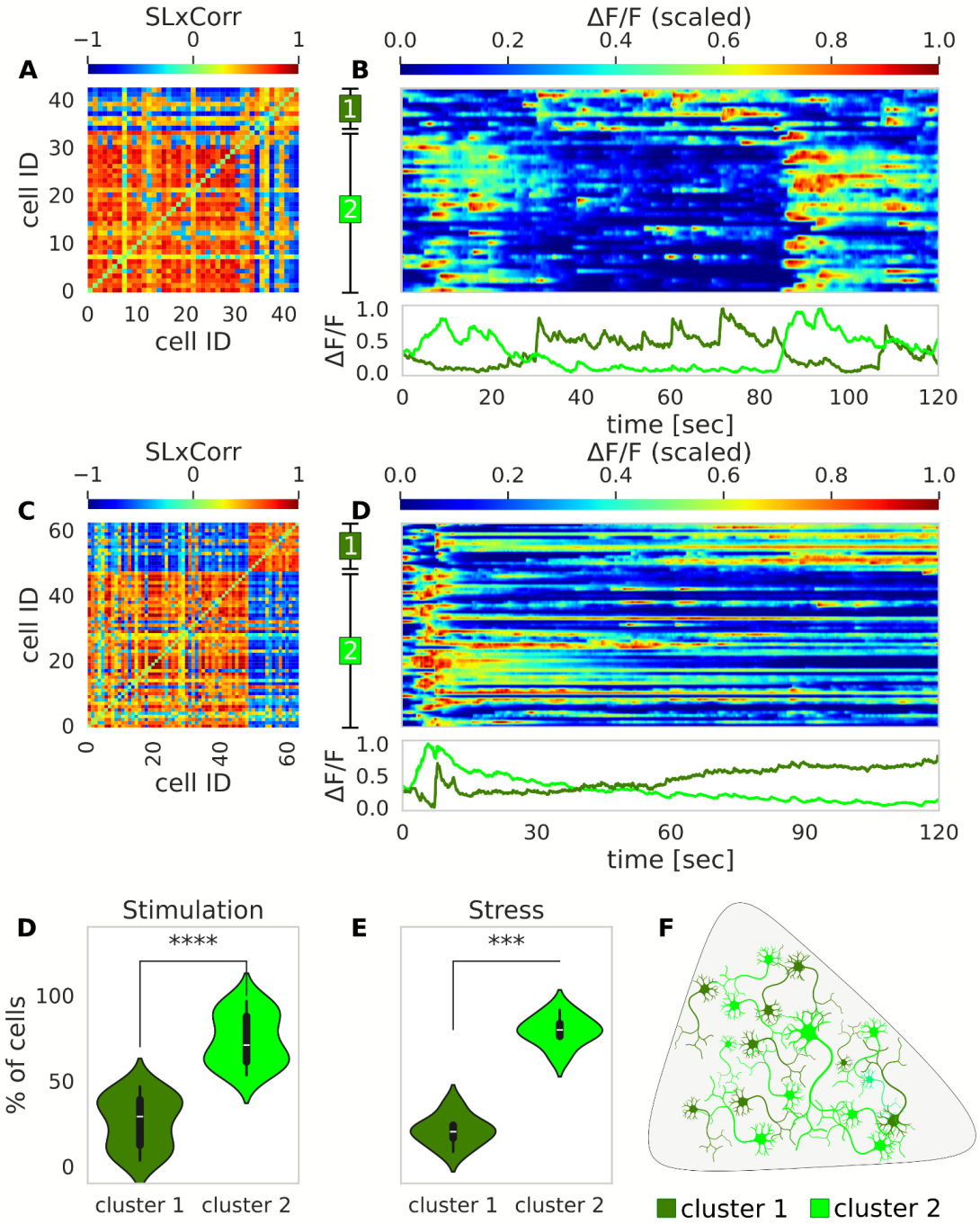

Figure 2: **Clustering identifies two functionally distinct GABAergic subpopulations in the posterodorsal medial amygdala (MePD) both during UCN3 optical stimulation and restraint stress**. Representative example of (**A**) a clustered connectivity matrix and (**B**) associated calcium time-traces of MePD GABA neurons during optical stimulation of UNC3 neurons and restraint stress. Representative example (**C**) of a clustered connectivity

matrix and (**D**) associated calcium activity time-traces of MePD GABA neurons during restraint stress. (**E**&**G)**. Relative sizes of the two GABAergic subpopulations identified via clustering analysis. (**** P<0.001).

Mutually inhibitory Interactions Between GABA Populations Drive Anti-Correlated Activity

To explore the functional role of the two GABAergic subpopulations identified through clustering analysis and unpick the mechanisms driving their anti-correlated activity, we build upon our previously developed MePD circuitry mathematical modelling framework[5]. The model captures the dynamics of intracellular calcium activity in subpopulations of GABA neurons (we refer to them as interneurons and efferent neurons) that interact with a glutamatergic neuronal population (Fig. 3**A**). Glutamate antagonism has been shown to completely block the suppressive effect of MePD UCN3 activation on LH pulsatility[10], suggesting a functional importance of glutamatergic neurons in the circuit, hence we keep this neuronal population in the model. To incorporate the effect of UCN3 input, we use recordings of the activity of UCN3 neurons during optogenetic stimulation (Fig. 3**A**). The recorded traces exhibit a periodic pattern driven by the experimental stimulation protocol with the cycle period of 10 sec (see Methods). In the model, we approximated this UCN3 input using a sinusoidal function with the same cycle period of 10 sec, driving the populations GABAergic interneurons and the glutamatergic neurons. We find that in order to reproduce anti-correlated activity between the two GABA neuronal subpopulations in the model we need to include bi-directional (i.e. mutually inhibitory) GABA interaction in the circuit as well as GABA interneurons self-inhibition (Fig. 3**A**).

Secondly, we simulate the effects of stress on the MePD circuit. UCN3 neurons in the MePD have also been shown to mediate psychosocial stress-induced suppression of the GnRH pulse generator[15]. Using our mathematical model we begin by reproducing experimental observations of GABA activity under an acute (120 sec) stress intervention (Fig. 3**B**). Experimentally recorded calcium activity of UCN3 neurons during stress intervention is characterised by a fast rise followed by a slow decay (Fig. 3**B**), which we model by taking the difference between two exponential functions, one with a fast and one with a slow time constant (see Methods). The model confirms emergence of anti-correlated behaviour between the GABAergic subpopulation whereby the activity of GABA interneurons decreases over the stress period,

while the activity of the GABA efferent neuron population increases (Fig. 3**B**), supporting the proposed MePD circuit structure (or connectivity).

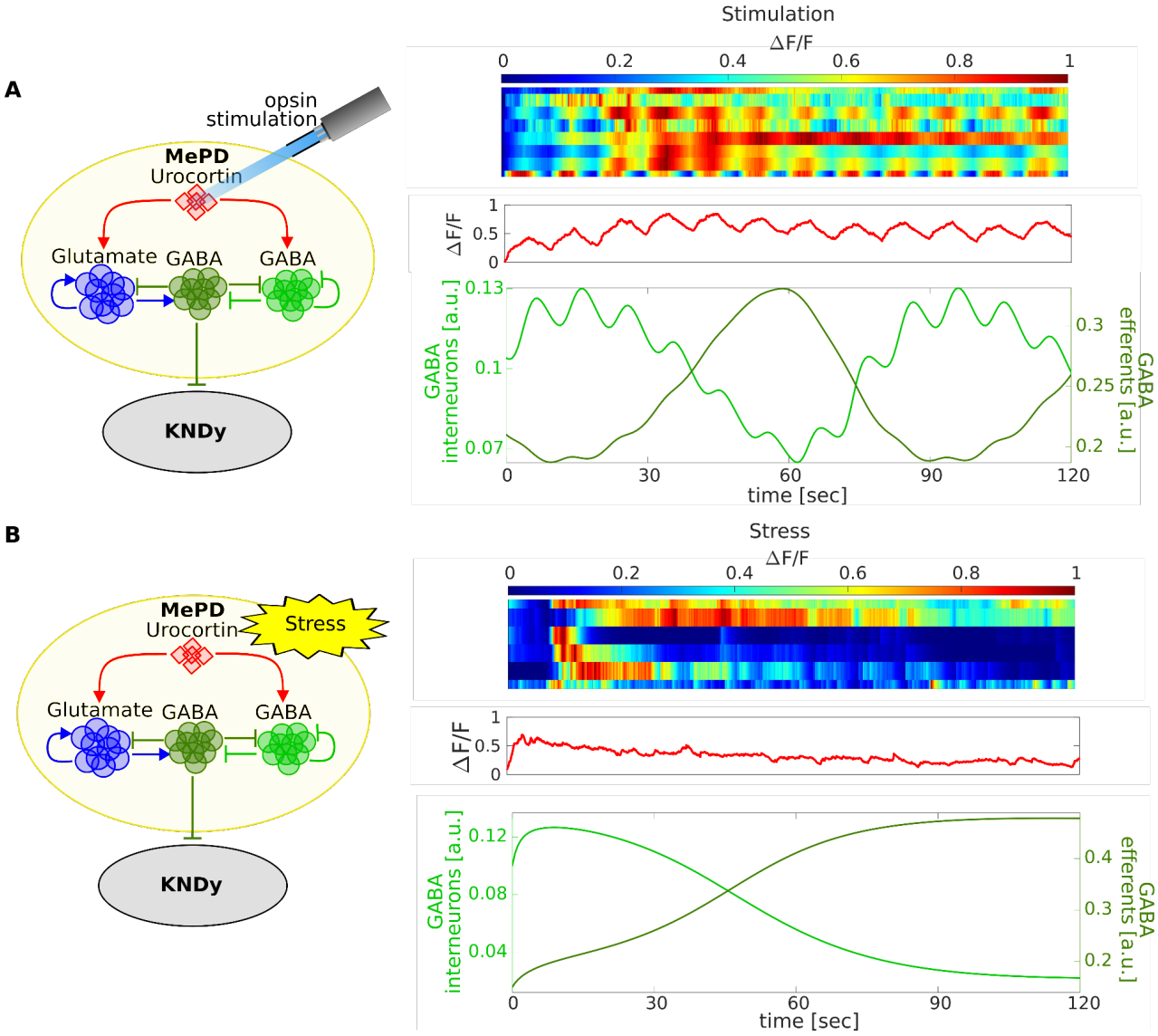

Figure. 3. ***In-silico* simulation of the activity in the GABAergic neuronal populations in the MePD under the increased excitatory input from UCN3 neurons and under restraint stress.** Schematic on the left representing the MePD neuronal circuit interacting with UCN3, consisting of two GABA populations and a glutamatergic population. (**A**) Calcium time-traces of MePD UCN3 neurons during optical stimulation of UNC3 neurons and corresponding mean activity. Model simulations of the effects of UCN3 optogenetic stimulation supports the emergence of anti-correlated activity in GABAergic subpopulations. (**B**) Calcium time-traces of MePD UCN3 neurons during optical stimulation of UNC3 neurons and corresponding mean activity of the UCN3 calcium traces

during restraint stress with corresponding mean activity. Simulations of the MePD circuit under the effects of stress also support anti-correlated GABAergic subpopulations' activity.

In-Silico Modelling Reveals Complementary Relationship between MePD GABA and UCN3 Populations

To examine the effects of distinct interventions of GABA and UCN3 in the MePD on the LH pulses we couple the model of the MePD circuitry to our network model of the KNDy population in the arcuate nucleus (ARC)[5,16]. Building on our previous *in-silico* findings, which suggest that MePD signal integration is mediated by GABAergic projections[5], here only the output from GABA efferent neuron populations is fed into the KNDy network. The effects of GABA and glutamate antagonism alone and together with UCN3 stimulation have been investigated[10]. We calibrate our coupled model by reproducing these effects on the LH pulsatility accordingly (Supplementary figure 1), thus calibrating our coupled model parameters.

Using the calibrated model we predict that providing a periodic excitatory input, that simulates the effects of optogenetic stimulation of UCN3, leads to the increase in the KNDy inter-pulse interval (IPI) from 15.73 min to 23.96 min due to increased activity in the inhibitory GABAergic input to the KNDy network (Fig. 4**A**).

Similar effect is predicted by simulating GABA neuronal populations' optogenetic stimulation, where we predict KNDy IPI increases from 15.73 min to 42.65 min (Fig. 4**B**). The MePD circuit connectivity assumes that both GABA populations inhibit each other almost with the same strength.

Then we inhibit the GABAergic populations by suppressing the strength of interactions by 50% and provide excitatory input to the circuit simulating the effects of UCN3 stimulation. The model shows that this intervention does not have a significant effect on KNDy IPI, apart from slightly increasing it from 15.73 min to 17.31 min (Fig. 4**C**).

Below we summarise our model predictions and suggest ways to test them experimentally:

1. Optogenetic stimulation modelled via excitation of the MePD UCN3 increases the KNDy IPI 15.73 min to 23.96 min. This could be tested experimentally via optogenetic activation of the MePD UCN3 neuronal populations;

2. Stimulation of the MePD GABA populations increases the KNDy IPI 15.73 min to 42.65 min. Such a substantial change underscores critical role of GABAergic signalling in modulating KNDy pulsatility. Experimental conformation could involve optical activation of the entire MePD GABAergic population;
3. Stimulation of the MePD UCN3 with simultaneous suppression of the GABAergic interactions in the circuit does not significantly affect KNDy IPI, changing it from 15.73 min to 17.31 min. This finding suggests that UCN3 effects on the KNDy network are primarily dependent on its interactions with GABA populations. This could be tested experimentally via enabling simultaneous optical stimulation of UCN3 non-GABA-expressing neurons and inhibition of non-UCN3 GABAergic neurons.

Taken together, these findings highlight the central role of GABA neuronal populations in UCN3-driven modulation of the KNDy network, offering experimentally testable predictions to further elucidate the role of UCN3 and GABA neurons in the circuitry.

Finally, we investigate *in-silico* the effects of stress on LH pulse dynamics mediated via the MePD. In the restraint-stress experiment it was shown that one GABAergic cluster was active, while the other one was inactive (Fig. 2**D**). By simulating these dynamics in the coupled MePD-KNDy model we are able to demonstrate that pulses in the KNDy network ceased (Fig. 4**D**). These findings align with experimental evidence indicating that restraint stress suppresses LH pulsatility[15].

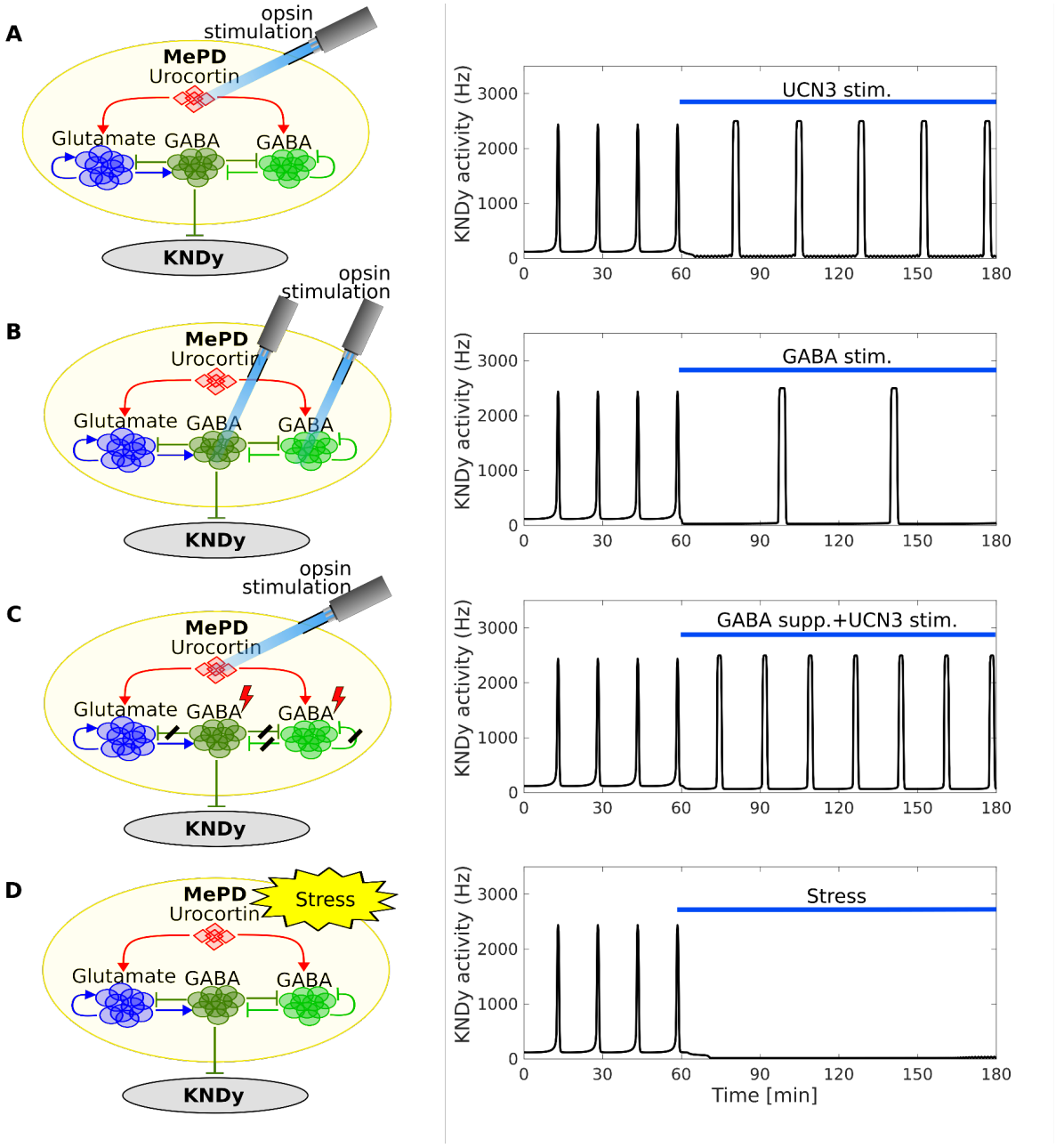

Figure. 4 | Coupled MePD-KNDy model predictions for the effect of UCN3 optical stimulation and stress on GnRH pulse generator activity and hence LH pulsatility. (**A**) Simulation of the optogenetic stimulation of the UCN3 neurons leads to the increase of the KNDy IPI 15.73 min to 23.96 min. (**B**) Optogenetic stimulation of the MePD GABA neurons (providing excitatory input to both GABAergic populations) increases KNDy IPI from 15.73 min to 42.65 min. (**C**) Optogenetic stimulation of the UCN3 neurons and simultaneous inhibition of GABAergic neuronal populations do not significantly affect KNDy IPI, where it changes from 15.73 min to 17.31 min. (**D**) Simulating the effects of stress leads to the cessation of the pulsatile dynamics.

Selective optical stimulation of UCN3 non-GABAergic neurons inhibits pulsatile LH secretion in female mice.

We experimentally test our modelling predictions detailed in the previous section regarding the inhibitory effect of MePD UCN3 activation on LH pulsatility. To this end a cohort of UCN3-Cre::VGAT-Flpo transgenic female mice was injected with an AAV-nEF-Con/Foff 2.0-ChRmine-oScarlet viral construct . This intersectional approach enabled conditional expression of channelrhodopsin (ChRmine) in UCN3 neurons not expressing GABA (UCN3 non-GABAergic) (Con/Foff group). Following the viral injection, a unilateral fiber-optic cannula was implanted into the MePD, above the injection site, to facilitate selective activation of the targeted neuronal population.

The stimulation protocol consisted of a 60-min control period, followed by 60 min of optical stimulation. Stimulation was delivered in a pulsed pattern (5 seconds on, 5 seconds off) with a pulse frequency of 10 Hz during the on period (10-ms pulse width, 10 mW power, 532 nm wavelength). Blood samples (5 μL) were collected every 5 min throughout the protocol and analysed for LH using ELISA.

In the Con/Foff group, the LH inter-pulse interval significantly increased after optical stimulation compared to the control period (15.33 ± 0.83 min vs. 23.75 ± 1.07 min, mean ± SEM, $n = 6$, $p < 0.01$; Fig. 5**A&D**), validating our modelling prediction 1. In contrast, the no-stimulation group, which received the Con/Foff viral construct without optical stimulation, showed no significant changes in LH inter-pulse interval (16.11 ± 0.56 min vs. 16.70 ± 0.96 min, $n = 3$, $p > 0.05$; Fig. 5**B&D**). Similarly, in a separate cohort of mice injected with a control virus (DIO-EYFP), optical stimulation resulted in no significant differences in LH inter-pulse intervals before and after stimulation (18.33 ± 1.18 min vs. 17.08 ± 1.25 min, $n = 4$, $p > 0.05$; Fig. 5**C&D**).

Selective optical stimulation of UCN3-expressing GABA neurons fails to affect pulsatile LH secretion in female mice.

To further test the functional interactions between the UCN3 and GABAergic populations, we employed an intersectional strategy. A separate cohort of UCN3-Cre::VGAT-Flpo transgenic female mice injected with an AAV-nEF-Con/Fon 2.0-ChRmine-oScarlet viral construct, which allows optogenetic stimulation of UCN3 neurons co-expressing GABA (UCN3-expressing GABA) (Con/Fon group). In the Con/Fon group,

LH inter-pulse intervals showed no change following optical stimulation compared to the control period (17.92 ± 0.80 min vs. 16.60 ± 0.88 min, mean ± SEM, n = 6, p > 0.05; Fig. 5**H&J**). Similarly, in the no-stimulation experiment for this cohort, which did not receive optical stimulation, there was no significant difference in LH inter-pulse intervals (15.42 ± 2.53 min vs. 15.83 ± 1.67 min, n = 3, p > 0.05; Fig. 5**I&J**).

Taken together, our results suggest that UNC3 and GABAergic populations are functionally orthogonal in the MePD circuit, i.e., activation of UCN3 neurons relay inhibitory information to the hypothalamic GnRH pulse generator but activation of the UCN3 neurons that co-expressing GABA are not sufficient.

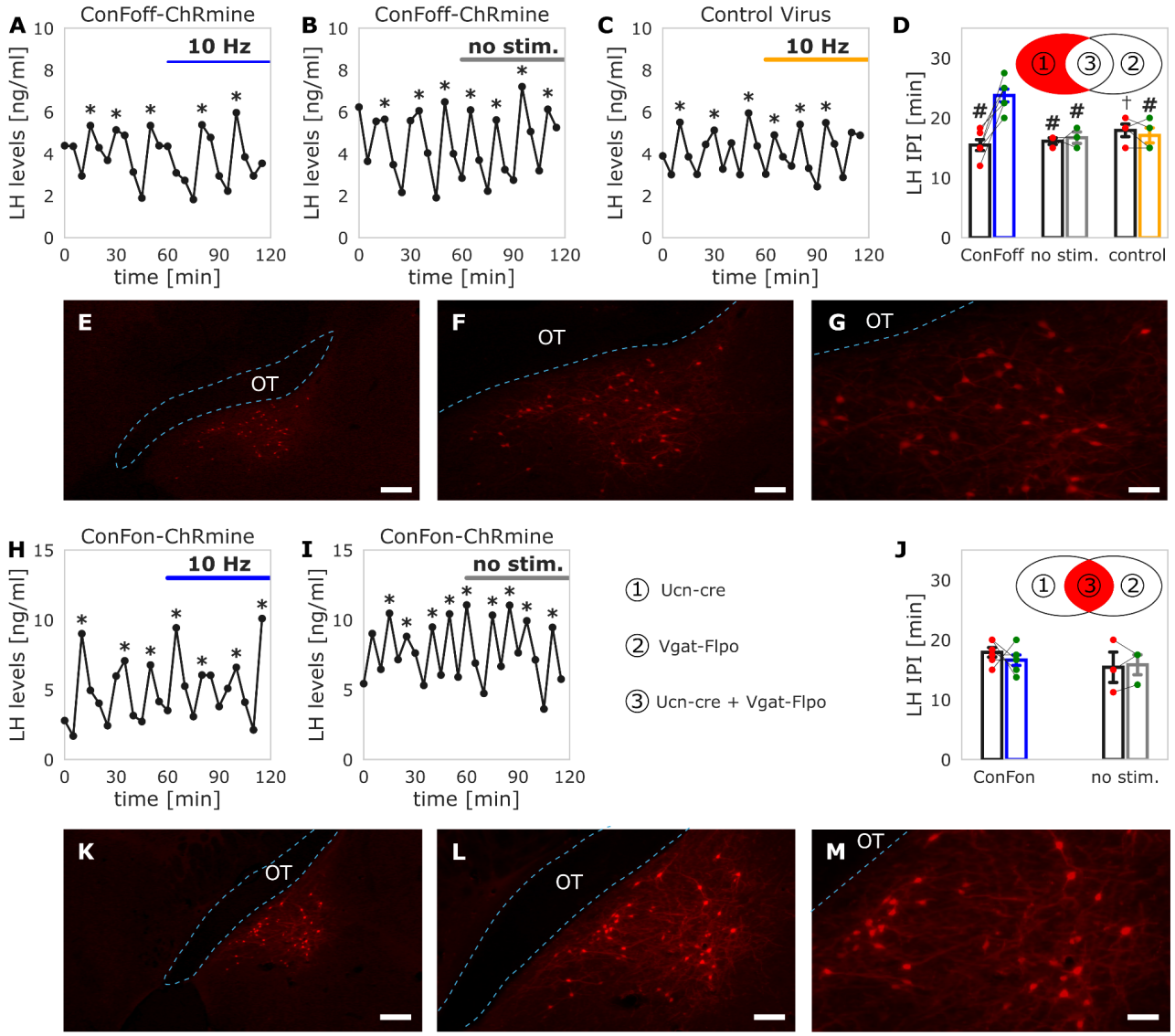

Figure 5. Effect of selective optical stimulation of UCN3 non-GABAergic and UCN3 neurons co-expressing GABA in the posterodorsal medial amygdala (MePD) on LH pulse frequency. Representative examples showing LH secretion in response to: (**A**) 10Hz optical simulation (532 nm wavelength, 10mW, 5 seconds on 5 seconds off, 10-ms pulse width) of UCN3 non-GABAergic neurons using a Con/Foff-ChRmine viral construct, (**B**) no stimulation as control, and (**C**) 10Hz optical stimulation using a control virus. LH pulses detected by the DynePeak algorithm are indicated with an asterisk (*). (**D**) Mean LH inter-pulse interval (IPI) (±SEM) for each group during the control period and over the subsequent stimulation period or equivalent. # P<0.01, † P<0.05 vs optical stimulated period in Con/Foff group; n=3-6 per group. (**E-G**) Representative photomicrographs of the MePD from a UCN3-Cre::VGAT-Flpo mouse injected with AAV-nEF-Con/Foff 2.0-ChRmine-oScarlet, with red fluorescence (oScarlet) indicating UCN3 non-GABAergic neurons expressing ChRmine. (**H-I**) Representative examples showing pulsatile LH secretion in response to (**H**) selective optical simulation at 10Hz (532 nm wavelength, 10mW, 5 seconds on 5 seconds off, 10-ms pulse width) of UCN3-expressing GABAergic neurons using a Con/Fon-ChRmine viral construct, and (**I**) no stimulation as control. (**J**) LH IPI summary statistics (mean±SEM) for each group during the control period and over the subsequent stimulation period. (**K-M**) Representative photomicrographs of the MePD from a UCN3-Cre::VGAT-Flpo mouse injected with AAV-nEF-Con/Fon 2.0-ChRmine-oScarlet, with UCN3-expressing GABA neurons displaying ChRmine are labeled with red fluorescence (oScarlet). OT, optic tract. Scale bars: E and K, 200μm; F and L, 100μm; G and M, 50μm.

The MePD GABAergic neurons relay information from UCN3 neurons and inhibit the GnRH pulse generator.

To test our model prediction and establish the functional role of GABAergic neurons in the MePD in transmitting inhibitory signals to the hypothalamic GnRH pulse generator, we injected the AAV-EF1a-ChR2 viral construct into VGAT-cre transgenic mice, targeting the entire MePD GABA neuron population for expressing ChR2. Using the previously described optical stimulation protocol (60 min control period followed by 60 min stimulation), activation of the entire MePD GABAergic population markedly increased the LH inter-pulse interval compared to the pre-stimulation control period (18.5 ± 2.03 min vs 49.5 ± 8.46 min, mean ± SEM, n = 5, p < 0.01; Fig. 6**A**&**D**), validating modelling prediction 2. In contrast, mice that did not receive optical stimulation showed no change in LH inter-pulse interval (23.13 ± 4.25 min vs 20.00 ±

1.77 min, n = 4, p > 0.05; Fig. 6**B**&**D**). Similarly, control virus (AAV-EF1a-DIO-EYFP) injections did not result in any significant difference in LH inter-pulse interval before and during optical stimulation (15.83 ± 0.83 min vs 18.33 ± 0.96 min, n = 3, p > 0.05; Fig. 6**C**&**D**).

Next, UCN3-Cre::VGAT-Flpo transgenic females were injected with an intersectional viral mixture containing AAV-nEF-Con/Foff 2.0-ChRmine-oScarlet and pAAV-nEF-Coff/Fon-NpHR3.3-EYFP , enabling simultaneous optical stimulation of UCN3 non-GABA neurons and inhibition of non-UCN3 GABAergic neurons. In this ConFoff+CoffFon group, optical stimulation did not produce any significant change in the LH inter-pulse interval relative to the control period (16.67 ± 1.31 min vs 18.61 ± 1.58 min, mean ± SEM, n = 6, p > 0.05; Fig. 6**H**&**J**), which aligns with our modelling prediction 3. Similarly, in mice injected with the same viral mixture but without receiving optical stimulation, no significant change in LH inter-pulse interval was detected (16.39 ± 2.47 min vs 16.67 ± 0.83 min, n = 3, p > 0.05; Fig. 6**I**&**J**).

Collectively, these findings suggest that MePD GABAergic neurons are integral to regulating LH pulse frequency. The inhibitory effect on LH pulses observed upon UCN3 neuron activation is attenuated when GABAergic neuron activity is optogenetically suppressed, implying that GABAergic signaling acts downstream of UCN3 neurons, relaying the inhibitory signal to the hypothalamic GnRH pulse generator.

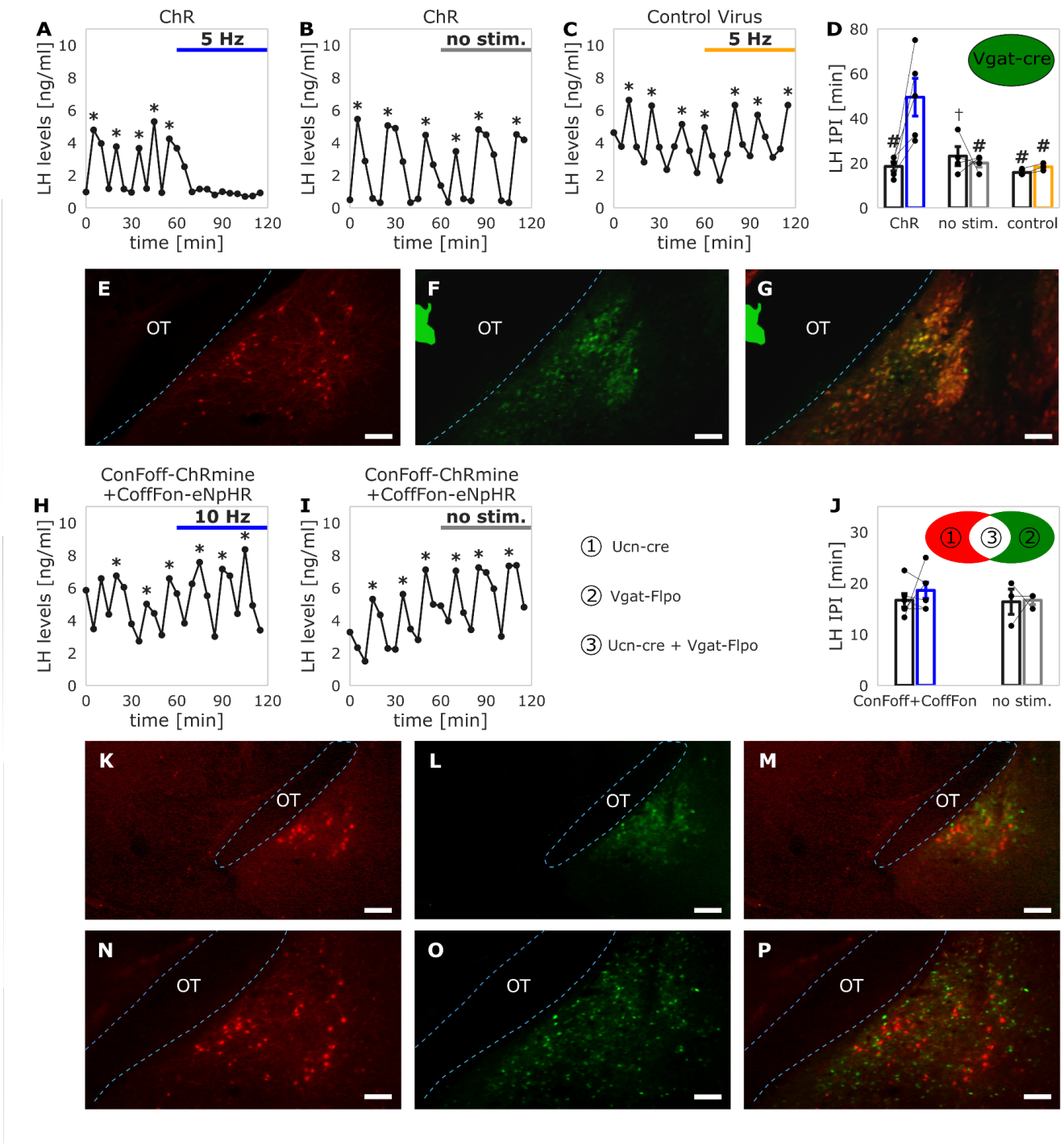

Figure. 6 | Selective optical stimulation of GABA neurons in the posterodorsal medial amygdala (MePD) inhibits LH pulsatility and their activity is necessary for mediating UCN3 signalling downstream. Representative examples showing LH secretion in response to (**A**) 5Hz optical simulation (473 nm wavelength, 5Hz, 5 seconds on 5 seconds off, 5mW, 10-ms pulse width) of GABA neurons in Vgat-Cre mice injected with a channelrhodopsin (ChR2) viral construct, (**B**) no stimulation as control, and (**C**) 5Hz stimulation using a control virus.

LH pulses detected by the DynePeak algorithm are indicated with an asterisk (*). (**D**) Mean LH inter-pulse interval (IPI) (±SEM) for each group during the control period and over the subsequent stimulation period . # P<0.01, † P<0.05 vs optical stimulated period in ChR2 group. (**E-G**) Representative photomicrographs of the MePD from a Vgat-Cre mouse, where (**E**) red fluorescence (dtTomato) labels GABA neurons, (**F**) green fluorescence labels ChR2-expreesing neurons and (**G**) red and green signals merged indicating GABA neurons expressing ChR2. (**H&I**) Representative examples showing LH secretion in response to (**H**) 10Hz optical simulation (532 nm wavelength, 10mW, 5 seconds on 5 seconds off, 10-ms pulse width) of UCN3 non-GABAergic neurons (using a Con/Foff-ChRmine viral construct) with simultaneous optical inhibition of non-UCN3 GABAergic neurons (using a Coff/Fon-NpHR3.3 viral construct) (**I**) no stimulation as control. Pulses detected by the DynePeak algorithm are indicated with an asterisk (*). (**J**) Mean LH inter-pulse interval (IPI) (±SEM) for each group during the control period and over the subsequent stimulation period. (**K-P**) Representative photomicrographs of the MePD from a UCN3-Cre::VGAT-Flpo mouse injected with AAV-nEF-Con/Fon 2.0-ChRmine-oScarlet and pAAV-nEF-Coff/Fon-NpHR3.3-EYFP viruses. (**K&N**) UCN3 non-GABAergic neurons expressing ChRmine labeled with red fluorescence (oScarlet). (**L&O**) Non-UCN3 GABA neurons expressing NpHR3.3 labeled with EYFP. (**M&P**) Red and green signals merged indicating no overlap between the two populations. OT, optic tract. Scale bars: E-G 150µm; K-M, 200µm; N-P, 100µm.

Discussion

The posterodorsal subnucleus of the Medial Amygdala (MePD), is a critical regulator of reproductive function, relaying stress-related cues to the reproductive axis and eliciting well-documented responses on pubertal timing[6,7], sociosexual behaviour[8,9], as well as on LH secretion[10,11] and the GnRH pulse generator[3–5]. Here, to elucidate how stress signals are processed within the MePD and to characterize the underlying neuronal circuitry, we used GRIN lens mini-endoscopic calcium imaging to study, for the first time, the dynamic activity of MePD GABAergic and UCN3 neurons under acute restraint stress as well as the activity of GABAergic neurons in response to UCN3 activation. Functional network analysis of the imaging data revealed that acute restraint stress induces a functional reconfiguration of the GABAergic population, emphasizing the pivotal role of GABA neurons in encoding and transmitting stress information. A comparable reconfiguration was observed following optical stimulation of UCN3 neurons, suggesting that these two populations are co-involved in stress processing. Further clustering analysis of the calcium transients identified two distinct GABAergic subpopulations with anti-correlated activity. This

finding of two distinct populations is consistent with physiological and morphological studies of GABAergic neurons in the medial amygdala characterising them as either projecting cells or interneurons[17,18].

Building upon a previously developed computational model of the MePD circuit, we explored the neuronal pathways underlying stress processing. The model consists of a glutamatergic subpopulation and two GABAergic subpopulations—one comprising GABAergic interneurons, and the other GABAergic efferent neurons. Our analysis identified two conditions necessary for the anti-correlated activity between these GABAergic subpopulations, consistent with our experimental observations. First, mutual inhibition between the GABA subpopulations is required, where activation of one subpopulation suppresses the activity of the other. Second, if both subpopulations receive a shared input (e.g., from the glutamatergic population), their dynamics become entrained to that common stimulus, meaning that distinct input streams to each subpopulation are necessary for the observed anti-correlation. To satisfy this condition in our model, GABAergic interneurons receive inputs from UCN3 neurons, whereas the GABAergic efferent subpopulation receives inputs from glutamatergic neurons. This circuitry implies that stress information is processed along two key pathways (one glutamatergic and one GABAergic) and is integrated by the GABAergic efferent neurons. We note that alternative connectivity patterns—such as direct projection of UCN3 neurons to the GABA efferent population—also fit our experimental observations but did not reproduce previously published results on the effects of neuropharmacological perturbations in the MePD on LH pulsatility[10]. Finally, the model predicted the outcomes of optical manipulation of UCN3 and GABA neurons on LH pulsatility, which we verified using an intersectional genetic strategy, further validating our approach.

Consistent with model predictions, we showed that optogenetic activation of UCN3-expressing, non-GABAergic neurons suppresses LH pulses. This finding corroborates previous work demonstrating that LH pulses are inhibited by activation of UCN3 neurones[7,10] or administration of UCN3[15] in the MePD, and that such effects are attenuated by chemogenetic inhibition of UCN3 neurons or by antagonising corticotropin-releasing factor type 2 receptors (CRHR2)[15]. Thus, our findings further support the central role of UCN3 signalling in modulating both stress responses and reproductive function.

GABA is one of the primary inhibitory neurotransmitters in the nervous system[17]. Previous work has shown that GABAergic neurons in the MePD project to the ARC to regulate LH pulses and chemogenetic

inhibition of MePD GABA neurons attenuates stress-induced suppression of LH pulses[15]. In this study, we found that optogenetic activation of GABAergic neurons in the MePD leads to robust LH suppression, reinforcing the pivotal role of GABAergic signalling in stress-related reproductive dysfunction. Antagonising GABA receptors in the MePD can block UCN3-induced LH suppression[10], suggesting that GABAergic neurons function downstream of UCN3 signalling. However, this pharmacological approach lacks cell-type specificity, leaving open the possibility that UCN3 neurons themselves co-expressing GABA receptors, potentially contributing to the observed effect. Here, by using an intersectional genetic strategy, we demonstrated that non-UCN3, GABAergic neurons can abolish the change in LH pulse intervals induced by optogenetic stimulation of UCN3 neurons, providing clear evidence that GABAergic neurons act downstream of UCN3 signalling in mediating LH suppression.

It is not unusual for neurons to co-express neuropeptides and neurotransmitters[18]. Given that activating either UCN3 or GABAergic neurons independently suppresses LH pulses, one might predict that stimulating neurons co-expressing both UCN3 and GABA would similarly inhibit LH. However, we observed no significant changes in LH pulses upon optogenetic stimulation of neurons co-expressing UCN3 and GABA. This suggests the two populations are functionally orthogonal: although both are essential for LH pulse inhibition, their overlap is not. Within our modeling framework, UCN3/GABA co-expressing neurons might be considered part of the GABAergic interneuron population, primarily inhibiting GABA projection neurons rather than activating them. Consequently, they fail to relay the inhibitory UCN3 signal to the ARC. Further studies are necessary to define more precisely the distinct roles and interactions of these two GABAergic subpopulations.

Methods

Animal

Vgat-cretdTomato mice were genotyped using PCR to determine heterozygosity for Vgat-cre (primers 5′-3′: common, 12785—CTTCGTCATCGGCGGCATCTG; wild-type reverse12786—CAGGGCGATGTGGAATAGAAA; mutant reverse oIMR8292—CCAAAAGACGGCAATATGGT) and tdtomato (primers 5′-3′: wild-type forward oIMR9020—AAGGGAGCTGCAGTGGAGTA; wild-type reverse oIMR9021—CCGAAAATCTGTGGGAAGTC; mutant reverse WPRE oIMR9103—

GGCATTAAAGCAGCGTATCC; mutant forward tdTomato oIMR9105—CTGTTCCTGTACGGCATGG). UCN3-Cre heterozygous mice (strain Tg(Ucn3-cre)KF43Gsat/ Mmucd, MMRRC GENSAT) were crossbred with VGAT-Flpo heterozygous mice (Jax stock #007909,B6.Cg-Slc32a1 2A-Flpo-D:Het) to obtain female double heterozygous UCN3-Cre::VGAT-Flpo mice (Slc32a1 2A-Flpo-D:Het|Ucn3-Cre:Het|Rosa26<tomato>WT); genotyped using PCR for the detection of heterozygosity (primers 5′- 3′: UCN3 Forward: CGAAGTCCCTCTCACACCTGGTT; Cre Reverse: CGGCAAACGGAC-AGAAGCATT; Slc32a1 Mutant Forward: TGC ATC GCA TTG TCT GAG TAG; Slc32a1 Mutant Reverse: GAC AGC CGT GAA CAG AAG G). Female mice, aged 8 to 10 week, weighing between 20g and 25g, were individually housed in ventilated cages sealed with a HEPA-filter at 25 ± 1°C in a 12:12-hour light/dark cycle, lights on at 07:00 h. Vaginal smears were performed when mice are 6 weeks old between 10:00 - 12:00 h daily. Only mice showing regular estrous cycles were included. All animal procedures performed were approved by the King's College London Animal Welfare and Ethical Review Body. Procedures were in accordance with UK home office regulation.

Stereotaxic Injection of Adeno-Associated Virus Construct and Fiber-Optic or Mini-Endoscope GRIN lens Implantation

All surgical procedures were carried out under general anaesthesia using ketamine (Vetalar, 100 mg/kg, i.p.; Pfizer, Sandwich, UK) and xylazine (Rompun, 10 mg/kg, i.p.; Bayer, Leverkusen, Germany) under aseptic conditions. Animals were secured in a David Kopf stereotaxic frame (Model 900, Kopf Instruments[KO1] , CA, USA). Following bilateral ovariectomy, a midline incision was made in the scalp to reveal the skull. Two small bone screws were inserted into the skull. A small hole was drilled above the position of the MePD. The MePD coordinate (2.29mm lateral, 1.60mm posterior from bregma, at a depth of 5.33mm below the skull surface) was determined according to the mouse brain atlas of Paxinos and Franklin[19]. A unilateral stereotaxic viral injection was performed to target opsin or fluorescent protein expression in the MePD neurons, using a robot stereotaxic system (Neurostar, Tubingen, Germany), with a 5-μL Hamilton microsyringe (Esslab, Essex, UK), at the speed of 25 nl/min for 10 min.

Two transgenic animal models were used for LH blood sampling under optical stimulation experiments: UCN3-Cre::VGAT-Flpo and VGAT-Cre-tdTomato. The following types of viral constructs were used in separated cohorts of UCN3-Cre::VGAT-Flpo mice: (i) AAV-nEF-Con/Foff 2.0-ChRmine-oScarlet (250nl, 2.1×10^{12} gc/mL, Serotype:8, #137161, Addgene, Massachusetts, USA); (ii) AAV-nEF-Con/Fon 2.0-ChRmine-oScarlet (250nl, 1.9×10^{12} gc/mL, Serotype:8, # 137159, Addgene, Massachusetts, USA); (iii) a mixture of AAV-nEF-Con/Foff 2.0-ChRmine-oScarlet (2.1×10^{12} gc/mL, #137161) and pAAV-nEF-Coff/Fon-NpHR3.3-EYFP (1.9×10^{12} gc/mL; #137159, final volume 300nl); (iv) control virus AAV-Ef1a-DIO-EYFP (250nl, 4.4×10^{12} gc/mL, Serotype:9, #27056, Addgene, Massachusetts, USA). VGAT-Cre-tdTomato mice received unilateral injections of (i) channelrhodopsin (ChR2) viral construct, (250nl, 1.8×10^{12} gc/mL; Serotype:9; Addgene, #20298, Massachusetts, USA) or (ii) control virus, AAV-Ef1a-DIO-EYFP (250nl, 4.4×10^{12} gc/mL, Serotype:9; Addgene, # 27056, Massachusetts, USA) into the MePD. Following injection, the needle was kept in position for 10 min before going up slowly over 1 min. A unilateral fibre optic cannula (200 µm, 0.39 NA, 1.25 mm ceramic ferrule; Doric Lenses, Quebec, Canada) was inserted into the right MePD 0.15 mm above the injection site. After reaching the target, the fibre optic cannula was secured on the skull using dental cement (Super-Bond Universal Kit, Prestige Dental, UK), bonded to the screws and skull. Finally, the incision in the scalp was closed with suture. Animals were given 1 week to recover, after which they were handled 20 min daily to acclimatise to experimental procedures for a further 2 weeks.

For mini-endoscope *in-vivo* calcium imaging, only UCN3-Cre::VGAT-Flpo transgenic animals were used. Separate mice cohorts received the following viral injection into the MePD: (i) a mixture of pAAV-Syn-Flex-rc[Chrimson-tdTomato] (2.0×10^{12} gc/mL, Serotype:5, #62723, Addgene, Massachusetts, USA) + pAAV-EF1a-fDIO-GCaMP6s (2.3×10^{12} gc/mL; Serotype:8; #105715, Addgene, Massachusetts, USA; final volume 400nl); (ii) a mixture of pAAV-Syn-Flex-rc[Chrimson-tdTomato] (2.0×10^{12} gc/mL, Serotype:5, #62723, Addgene, Massachusetts, USA) + pAAV.CAG.Flex.GCaMP6s.WPRE.SV40 (4.3×10^{12} gc/mL; Serotype:9; # 100842, Addgene, Massachusetts, USA; final volume 400nl); (iii) a mixture of control virus AAV-Ef1a-DIO-EYFP (250nl, 4.4×10^{12} gc/mL, Serotype:9, #27056, Addgene, Massachusetts, USA) + pAAV-EF1a-fDIO-GCaMP6s (2.3×10^{12} gc/mL; Serotype:8; #105715, Addgene, Massachusetts, USA; final volume 250nl). One week after administering the virus, a 600-µm

diameter, 7.2-mm long gradient index (GRIN) ProView™ Integrated Lens (Inscopix, PN:100-004554) was implanted at the same location as the viral injection. The surface of the skull was scored, using the tip of a surgical scalpel, and four screws were inserted into the skull. This was done to enhance the adhesion of dental cement to the skull, thereby reducing the interference of movement on *in-vivo* recording. Before insertion of the GRIN lens, a 23 G needle was slowly lowered at a speed of 5.0mm/min into the brain (2.42mm lateral, 1.52mm posterior from bregma, depth of 5.05mm below the skull surface) to make a needle track to facilitate the insertion of the GRIN lens without causing brain distortion along its route. The GRIN lens was then inserted into the brain at a rate of 0.6 mm/min, using the same coordinates as the needle precutting. T To secure the GRIN lens with integrated baseplate in position, we used a light curing adhesive (iBond Universal, Kulzer GmbH, Leipziger, Germany, Ref:66061411) along with a cured radiopaque hybrid dental cement (Gradia Direct Flo, GC corporation, Tokyo, Japan, Ref:002278), bonding it to the head screws and skull. A GRIN lens baseplate dust cover (Inscopix) was rescued in place to protect the lens. After four weeks the mice were re-anaesthetised as described above and underwent bilateral ovariectomy.

Serial tail blood sampling

The mouse's tail-tip was excised using a sterile scalpel. Then the chronically unilaterally implanted fibre optic cannula was connected to a multimode fibre optic rotary joint patch cables (Thorlabs Ltd, Ely, UK) via a ceramic mating sleeve to allow the animal freedom of movement. Mice were left for 1 hour to habituate. A Grass SD9B stimulator-controlled DPSS laser (Laserglow Technologies, Toronto, Canada) was utilised to deliver either green light (532 nm wavelength, 10Hz, 5 seconds on 5 seconds off, 10mW, 10-ms pulse width,) or blue light (473 nm wavelength, 5Hz, 5 seconds on 5 seconds off, 5mW, 10-ms pulse width,). The optical stimulation pattern was controlled using software designed in house. After an hour of acclimatisation, serial blood samples (5-μL) for LH pulse measurement were collected every 5 min for 2 hours between 10:00 h and 12:00 h: 0-60 min for control blood sampling period, and 60-120 min under optical stimulation or equivalent no-stimulation control period. Blood samples were diluted in 45 μL of 0.2% BSA-0.05% PBS with Tween-20 (0.2% BSA and 0.05% PBST) and immediately placed on dry ice and stored at −80 °C until later analysis.

LH measurement

LH measurement was performed using an LH ELISA assay as reported previously[20]. A mouse LH standard (mLH; AFP-5306A, NIDDK-NHPP, USA) was used to establish a standard curve for the quantitative measurement. The following antibodies were used in the assay: (i) coating antibody (RRID: AB_2665514, monoclonal antibovine LH beta subunit antiserum, 518B7, University of California, CA, USA); (ii) anti-LH antibody (RRID: AB_2665533; National Hormone & Peptide Program, CA, USA); (iii) secondary antibody (RRID: AB_772206, GE Healthcare, Chicago, Illinois, USA). The inter-assay and intra-assay variations were 10.53% and 5.74 %, respectively. The assay sensitivity was 0.023 ng/mL.

LH pulse statistical analysis

LH pulses were verified using the Dynpeak algorithm in Scilab 5.5.2 programme[21]. The dynpeak algorithms were classified for OVX mice based on previously established parameters[22]. The average LH inter-pulse interval was calculated for the 1-hour control period and the 1-hour optical stimulation period in both experimental and control mice. Statistical significance was assessed using a 2-way ANOVA unless otherwise stated. Data was represented as mean ± SEM and $p < 0.05$ was considered significant.

Mini-Endoscope-based Calcium imaging

Under optogenetic stimulation of MePD UCN3 neurons. Prior to recording, animals were handled daily for 5 to 6 weeks to get accustomed to the experimental setup. The Data Acquisition (DAQ) box (Inscopix, PN:100-005904) was turned on and connected to the computer wirelessly. The Data Acquisition Software (IDAS; Inscopix, Inc.) was accessed through the Chrome web browser on the computer communicating with the DAQ box. Adequate DAQ box storage capacity was checked routinely before Calcium imaging. The GRIN lens baseplate dust cover was gently removed from the mouse's head, after which the minscope camera was secured to the baseplate platform. Equipped with the head-mount miniscope (nVoke2, Inscopix, SN: BB-11238601), the mouse was then placed back into its home cage. The optimal focal plane was chosen by adjusting the lens focus to achieve clear cell morphology. The exposure time was fixed at 50ms. The frame rate was set to 20Hz. Subsequently, gain, and LED power were optimised based on image histograms before initiating recording. Two types of LED were used during the recording: (i) EX-LED (0.2-0.4mW, 435-460 nm excitation filter) for GCaMP6s signal detection in the GABAergic or

UCN3 neurons; (ii) OG-LED (10mW, 590-650 nm excitation filter) for Chrimson optogenetic stimulation of the UCN3 neurons. After the mice were attached to the miniscope, they were given 1-2 hours for adaptation. For the optical stimulation of the UCN3 neurons, the OG-LED was set to 10Hz, 5 seconds on 5 seconds off, and a 10-ms pulse width. Once the animals had acclimatised, the GCaMP6s recording of the GABAergic neurons or UCN3 neurons was started with a protocol of 2 min baseline before optical stimulation, 2 min during optical stimulation, and 3 min post stimulation. Optogenetic stimulation was randomised for the 10Hz, with a 5-min interval between each to prevent photobleaching of GCaMP6s. Once the experiment was concluded, the miniscope was gently detached, and the baseplate cover was reattached and secured with its screw. The recordings were performed between 9:00 h and 15:00 h. Three groups of animals were included in this experiment: (i) mice with UCN3 neurons expressing opsin and GABAergic neurons expressing GCaMP; (ii) mice with UCN3 neurons expressing both opsin and GCaMP, serving as a positive control; (iii) mice with UCN3 neurons expressing mCherry and GABAergic neurons expressing GCaMP, serving as a negative control.

Under restraint stress. The system was set up and the mouse was connected to the miniscope as described above but with the OG-LED turned off. Once the mouse had settled, the experiment started with a three-minute baseline recording, followed by three minutes of recording under hand-held restraint. Finally, the miniscope was detached and the baseplate cover was reattached. The experiments were performed between 9:00 h and 15:00 h. The animals in this experiment were the same as those used in the optogenetic stimulation protocol described above but were divided into two groups depending on whether GCaMP was expressed in the UCN3 or GABAergic neurons, regardless of whether opsin or mCherry was expressed in the UCN3 cells.

In-vivo calcium imaging recording processing

The video data, with a resolution of 1280 pixels x 800 pixels, was exported from the DAQ box through the File manager to a desktop computer installed with the Inscopix Data Processing Software (IDPS) for processing. Within the IDPS, there are six essential steps: down-sampling, cropping, spatial filtering, motion correction, and ΔF/F calculation, aimed at extracting single-cell calcium transient data from the recorded video. The video underwent both spatial down-sampling and temporal down-sampling by a factor

of 2 and was cropped to enhance processing speed, focusing on the region of interest where the GCaMP signal was observed. Spatial filtering, with a threshold ranging between 0.005 (low) and 0.5 (high) was used to distinguish individual pixels in the video image, creating a high-contrast image. A mean intensity projection image was generated. Motion correction was subsequently conducted, utilising the mean intensity projection image as a reference. Motion correction was applied again using one of the frames affected by movement while simultaneously drawing a region of interest (ROI) where UCN3 accumulates to enhance the effectiveness of motion correction. For the recordings with GCaMP signals from GABAergic neurons, we did not use the built-in motion correction function of IDPS. Instead, we used the MATLAB (version R2022a) implementation of the open-source algorithm NoRMCorre[23] with default parameters for both rigid and non-rigid (patch size 64 pixels and overlap 32) motion correction as long as a minimum correlation of the frames with the mean frame above 0.8 is achieved. Occasionally, if the minimum correlation is not met, an extra step of non-rigid motion correction with coarser patches is applied. This is performed by doubling the patch size and their overlap to 128 and 64, respectively. Finally, the corrected videos are saved in TIFF format for further analysis via IDPS.

The changes in brightness were visualised using the ΔF/F calculation to detect calcium transients in pixels. The principal component analysis/independent component analysis (PCA/ICA) algorithm was utilised to visualise the calcium transient curve of each cell. Non-neuronal elements were manually removed based on criteria focusing on signals that indicate neuronal activity and sizes matching typical dimensions of neuron cell bodies. Cell traces were deconvolved using an OASIS method with a noise range between 0.25 and 0.5. Neurons with a minimum signal-to-noise ratio (SNR) >= 3 were included for further analysis.

Validation of virus injection, fibre optic cannula and GRIN lens implantation

Once the experimental procedures were completed, a lethal dose of ketamine was used to humanely euthanise the mice. The mice were perfused transcardially with heparinised saline (5 U/ml) for 5 min, followed by ice-cold 4% paraformaldehyde (PFA) for 15 min using a pump (Minipuls,156 Gilson, Villiers Le Bel, France). The brains were collected and post-fixed sequentially at 4℃ in a solution of 15% sucrose in 4% PFA and later in a solution of 30% sucrose in phosphate buffer until they sank. They were then

snap frozen on dry ice and stored in -80℃ until processing. The brains were coronally sectioned (30 μm) between +0.5 mm and -2.7 mm from the bregma using a cryostat (Bright Instrument Co., Huntingdon, UK), and sections were mounted on microscope slides, air-dried, and covered with slips using Prolonged Antifade mounting medium (Molecular Probes, Inc. OR, USA). The accuracy of injection sites, fibre optic cannula and GRIN lens implantation were confirmed by Axioskop 2 Plus microscope equipped with AXIOVISION 4.7 (Zeiss). Images were captured using Axioskop 2 Plus microscope (Carl Zeiss). Only the data of mice with correct viral infection and implantation of cannula and lens in the MePD were included in the analysis.

Data analysis

The data acquisition protocol analysed in this study consists of two phases: pre-intervention and intervention (either via optogenetic stimulation or stress). For our analysis, we use the smoothed deconvolved traces generated by the OASIS method[24], which improves the signal-to-noise ratio (SNR) and mitigates noise interference. All traces are rescaled between 0 and 1 (min-max normalisation), and then further normalised to mean zero and unit variance. The analysis process is divided into three key steps: i) identification of GABA cells co-expressing UCN3 and removing them from further analysis; ii) estimating and comparing functional connectivity before and during intervention; iii) clustering analysis based on functional connectivity

In step (i) we use power spectral density (PSD) analysis and K-means clustering (using Euclidean distance) to identify GABA neurons with activity that mimics the pattern of optic stimulation, evidence that they are co-expressing UCN3.

PSD Filtering. For each trace, we compute the PSD during the stimulation phase. Cells with PSD values at 0.1 Hz (the frequency of the stimulus 5 second on and 5 second off cycle) above 0.37 Hz^{-1} are labelled as coexpressing UCN3. This threshold is determined from recordings of UCN3 cells under optic stimulation, by calculating the median of the minimum PSD values at 0.1 Hz from each dataset.

K-means Clustering. Using the Euclidean distance metric, we cluster the traces during the stimulation phase into two groups, aiming to separate neurons into GABA-only neurons and neurons co-expressing

UCN3 and GABA. Clustering separated neurons with activity mimicking the optic stimulation oscillatory pattern as a small group (see Supplementary figure 2) that was labelled as coexpressing UCN3.

Neurons identified by either method as co-expressing UCN3 and GABA are excluded from further analysis. By applying both filters, we aim to robustly identify purely GABA-expressing neurons. We acknowledge the fact that due to limitations some cells may pass through the filters or that a few purely GABA-expressing neurons may be inadvertently excluded. Nevertheless, this process is essential to ensure our analysis remains focused exclusively on GABA-expressing neurons.

Comparing pre-intervention and intervention cell-cell interaction strength

Following step (i) the remaining dataset contains only traces associated with GABA neurons. In step (ii) we assess the functional connectivity between the observed neurons using two measures of association of their activity traces, namely covariance and a modified version of cross-correlation. The covariance between two traces $x = \{x_i\}$ and $y = \{y_i\}, i = 1, \dots, N$ is defined as

$$cov(x, y) = \frac{1}{N-1}\sum_i (x_i - \overline{x})(y_i - \overline{y}), \qquad \overline{x} = \frac{1}{N}\sum_i x_i, \qquad \overline{y} = \frac{1}{N}\sum_i y_i$$

quantifying the strength of their linear association[25].

The modified cross-correlation, also accounting for lag and sign in cell-cell interactions, is termed *signed lagged cross-correlation* (SLxCorr) and is adapted from the works of Tsuyuzaki et al.[26] and Paparrizos &Gravano[27]. It is defined as:

$$\mathrm{SLXCorr}(x, y) = \frac{R_{\tau_{max-N}}(x, y)}{\sqrt{R_0(x, x)R_0(y, y)}},$$

in which

$$\tau_{max} = \underset{\tau}{\mathrm{argmax}}\left(\left|\frac{R_{\tau-N}(x, y)}{\sqrt{R_0(x, x)R_0(y, y)}}\right|\right),$$

where $R_\tau = \begin{cases} \sum_{i=1}^{N-\tau-1} x_{i+\tau} \cdot y_i & \text{for} \quad \tau \geq 0 \\ R_{-\tau}(y, x) & \text{for} \quad \tau < 0 \end{cases}$ represents cross-correlation with lag $\tau \in \{-N + 1, \dots, -1, 0, 1, \dots, N-1\}$ with N is the length of x and y.

Using the above measures we construct covariance and SLxCorr matrices (Fig. 1).

To evaluate changes in pairwise cell interactions between the pre-intervention and intervention phases, we compare the covariance and SLxCorr matrices using the Kolmogorov-Smirnov nonparametric statistical test[28,29]. This test is applied to each trial with each metric independently. For each trial, only the upper triangular entries (excluding the diagonal) of the covariance and SLxCorr matrices are used to avoid duplication caused by the symmetry of cell interactions.

To account for variability across experimental conditions, we combine the p-values obtained from individual trials into a single p-value for each animal. This is done using Fisher's Combined Probability Test[30], providing an overall measure of the difference between the pre-intervention and intervention stages for each animal.

Clustering analysis

In step (iii) we apply agglomerative hierarchical clustering (using the average linkage criterion; scikit-learn package in Python™) and K-means to classify cells based on the similarity of their calcium activity.

To determine the optimal number of clusters and robustness of clustering we employed a bootstrapping technique. This involved resampling (without replacement) 75% of the cells and clustering the resulting dataset with different numbers of clusters (2, 3, and 4), using hierarchical or K-means clustering, with either the covariance or SLxCorr as the dissimilarity metric. This resampling process was repeated 100 times.

Modelling

We modify our previously published model of MePD circuit[5] in order to incorporate dynamic stimulation by UCN3 as observed experimentally (as shown in Fig. 3). Briefly, the model captures the dynamics of the MePD intracellular calcium activity of three populations: glutamatergic neuronal population (excitatory) and the populations of GABA interneurons and GABA efferent neurons (inhibitory). We build on our previous work[5] by assuming that excitatory (UCN3) input is provided to the populations of GABA interneurons and glutamate represents the input of the UCN3 (Fig 7). Previous analysis of the model indicated that negative feedback between GABAergic and glutamatergic neuronal populations as well as glutamatergic self-excitation are critical mechanisms for inducing oscillatory dynamics[5]. However, providing glutamatergic

input to both populations of GABA neurons causes the phase difference between the populations to become null. Therefore, we opted to provide glutamatergic input only to the population of GABA efferent neurons.

To investigate how the amygdala modulates the activity in the GnRH pulse generator, we couple the extended MePD model to the KNDy network, where the oscillatory dynamics of the KNDy acts as a proxy of LH pulsatility[16]. Here we couple the model via providing only inhibitory output from MePD GABA efferent neurons population to KNDy, as it was previously shown that glutamate plays a modulatory role to the MePD output rather than directly to KNDy[5]. We then used the coupled model to calibrate the model by reproducing the experimental results from Ivanova et al.[10] (Supplementary figure 1). Further modelling details can be found in Supplementary.

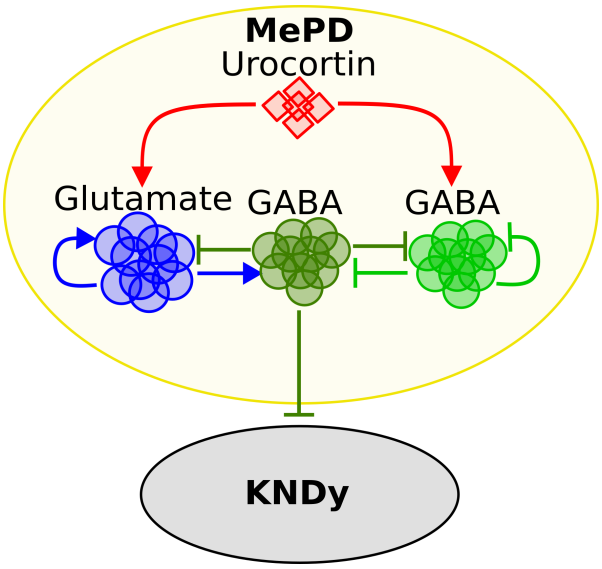

Figure 7: Schematic diagram of the GABA–glutamate circuit in the MePD. Urocortin (red) activates the populations of glutamate (blue) neurons and GABA interneurons (bright green). The population of GABA efferent neurons (dark green) functionally interacts with the glutamatergic population and the population of GABA interneurons. The activity within the GABAergic efferent neurons goes downstream to the ARC to modulate the activity of the KNDy population.

Data Availability

The data sets used in this study are available online at [King's/Exeter repository].

Code Availability

The Python™ notebooks for analysing the data and recreating the figures in the main manuscript and also supplementary materials along with a test data set are publicly accessible at https://github.com/SaeedF36/GABA.git.

References

1. Yeo, S.-H., Kyle, V., Blouet, C., Jones, S. & Colledge, W. H. Mapping neuronal inputs to Kiss1 neurons in the arcuate nucleus of the mouse. *PLOS ONE* **14** (2019).
2. Moore, A. M., Coolen, L. M. & Lehman, M. N. Kisspeptin/Neurokinin B/Dynorphin (KNDy) cells as integrators of diverse internal and external cues: evidence from viral-based monosynaptic tract-tracing in mice. *Sci. Rep.* **9** (2019).
3. Comninos, A. N. *et al.* Kisspeptin signaling in the amygdala modulates reproductive hormone secretion. *Brain Struct. Funct.* **221**, 2035–2047 (2016).
4. Lass, G. *et al.* Optogenetic stimulation of kisspeptin neurones within the posterodorsal medial amygdala increases luteinising hormone pulse frequency in female mice. *J. Neuroendocrinol.* **32** (2020).
5. Nechyporenko, K. *et al.* Neuronal network dynamics in the posterodorsal amygdala: shaping reproductive hormone pulsatility. *J. R. Soc. Interface* **21** (2024).
6. Adekunbi, D. A. *et al.* Role of amygdala kisspeptin in pubertal timing in female rats. *PLOS ONE* **12** (2017).
7. Ivanova, D. *et al.* Role of Posterodorsal Medial Amygdala Urocortin-3 in Pubertal Timing in Female Mice. *Front. Endocrinol.* **13**, (2022).
8. Adekunbi, D. A. *et al.* Kisspeptin neurones in the posterodorsal medial amygdala modulate sexual partner preference and anxiety in male mice. *J. Neuroendocrinol.* **30** (2018).
9. Wu, Y. E. *et al.* Neural control of affiliative touch in prosocial interaction. *Nature* **599**, 262–267 (2021).
10. Ivanova, D., Li, X.-F., McIntyre, C. & O'Byrne, K. T. Posterodorsal Medial Amygdala Urocortin-3,

GABA, and Glutamate Mediate Suppression of LH Pulsatility in Female Mice. *Endocrinology* **164**, 1–13 (2023).

11. McIntyre, C. *et al.* GABA Signaling in the Posterodorsal Medial Amygdala Mediates Stress-induced Suppression of LH Pulsatility in Female Mice. *Endocrinology* **164**, 1–11 (2023).
12. Choi, G. B. *et al.* Lhx6 delineates a pathway mediating innate reproductive behaviors from the amygdala to the hypothalamus. *Neuron* **46**, 647–660 (2005).
13. Lewis, K. *et al.* Identification of urocortin III, an additional member of the corticotropin-releasing factor (CRF) family with high affinity for the CRF2 receptor. *Proc. Natl. Acad. Sci. U. S. A.* **98**, 7570–7575 (2001).
14. Shemesh, Y. *et al.* Ucn3 and CRF-R2 in the medial amygdala regulate complex social dynamics. *Nat. Neurosci.* **19**, 1489–1496 (2016).
15. Ivanova, D. *et al.* Urocortin3 in the Posterodorsal Medial Amygdala Mediates Stress-induced Suppression of LH Pulsatility in Female Mice. *Endocrinology* **162**, 1–14 (2021).
16. Voliotis, M. *et al.* The Origin of GnRH Pulse Generation: An Integrative Mathematical-Experimental Approach. *J. Neurosci.* **39**, 9738–9747 (2019).
17. Keshavarzi, S., Sullivan, R. K. P., Ianno, D. J. & Sah, P. Functional Properties and Projections of Neurons in the Medial Amygdala. *J. Neurosci.* **34**, 8699–8715 (2014).
18. Bian, X. Physiological and morphological characterization of GABAergic neurons in the medial amygdala. *Brain Res.* **1509**, 8–19 (2013).
19. Paxinos, G. & Franklin, K. B. J. *Paxinos and Franklin's the Mouse Brain in Stereotaxic Coordinates*. (2019).
20. Steyn, F. J. *et al.* Development of a Methodology for and Assessment of Pulsatile Luteinizing Hormone Secretion in Juvenile and Adult Male Mice. *Endocrinology* **154**, 4939–4945 (2013).
21. Vidal, A., Zhang, Q., Médigue, C., Fabre, S. & Clément, F. DynPeak: An Algorithm for Pulse Detection and Frequency Analysis in Hormonal Time Series. *PLOS ONE* **7** (2012).
22. Yang, L. *et al.* The Effects of Kisspeptin on Brain Response to Food Images and Psychometric Parameters of Appetite in Healthy Men. *J. Clin. Endocrinol. Metab.* **106** (2021).
23. Pnevmatikakis, E. A. & Giovannucci, A. NoRMCorre: An online algorithm for piecewise rigid motion

correction of calcium imaging data. *J. Neurosci. Methods* **291**, 83–94 (2017).

24. Friedrich, J., Zhou, P. & Paninski, L. Fast online deconvolution of calcium imaging data. *PLOS Comput. Biol.* **13** (2017).
25. Rice, J. A. *Mathematical Statistics and Data Analysis*. (Thomson/Brooks/Cole, Belmont, CA, 2007).
26. Tsuyuzaki, K. *et al.* WormTensor: a clustering method for time-series whole-brain activity data from C. elegans. *BMC Bioinformatics* **24**, 254 (2023).
27. Paparrizos, J. & Gravano, L. k-Shape: Efficient and Accurate Clustering of Time Series. *SIGMOD Rec* **45**, 69–76 (2016).
28. Kolmogorov, A. Sulla determinazione empirica di una legge didistribuzione. *Giorn Dellinst Ital Degli Att* **4**, 89–91 (1933).
29. Smirnoff, N. On the estimation of the discrepancy between empirical curves of distribution for two independent samples. *Bull Math Univ Moscou* **2**, 16 (1939).
30. Fisher, S. R. A. *Statistical Methods for Research Workers*. (Oliver & Boyd, 1970).

Acknowledgements

We thank Ms Sumi Mathew for her technical support with genotyping mice.

BBSRC grant (BB/W005913/1) O'Byrne and Li.

Competing interests

The authors declare no competing interests.